



Novel uranyl-curcumin-MOF photocatalysts with highly performance photocatalytic activity toward the degradation of phenol red from aqueous solution: effective synthesis route, design and a controllable systematic study

Farideh Miri Khandan¹ · Daryoush Afzali^{1,2} · Ghasem Sargazi¹ · Mohammad Gordan³

Received: 29 May 2018 / Accepted: 31 August 2018 / Published online: 3 September 2018
© Springer Science+Business Media, LLC, part of Springer Nature 2018

Abstract

In this work, the uranyl-curcumin metal–organic framework (MOF) samples were synthesized using ultrasound, reflux, hydrothermal and ultrasound assisted reflux techniques. Fourier transform infrared spectroscopy, X-ray diffraction, thermogravimetric analysis, scanning electron microscopy, transmission electron microscopy, and N₂ adsorption/desorption isotherm were used to identify and investigate the properties of the samples. The results showed that the synthesized products by ultrasound methods shows excellent properties than the other methods and had a significant porosity of 2.74 nm with the surface area of 42.66 m²/g. In this method, the size of particles is in the range of 40–90 nm, and the samples had a spherical morphology by uniform distribution without any agglomeration. In the second part of this study, the 2^{k-1} factorial method was used to evaluate the effects of several parameters (pH, contact time, phenol red concentration and photocatalyst content) on the photocatalytic activity of the uranyl-MOF with curcumin ligands in the degradation of phenol red from aqueous samples. The results showed that in optimal conditions (pH 8.04, contact time: 11 min, phenol red concentration: 0.11 mg/L, and amount of MOF: 18.00 mg), more than 99% of the phenol red could be degraded.

1 Introduction

Metal–Organic framework (MOF) is a group of porous nanomaterials that have received special attention to their distinctive features over other nanostructures [1, 2]. Unique properties of these compounds are high chemical and thermal stability, ideal physicochemical properties and flexibility in design [3, 4].

These materials are synthesized by various methods under different conditions including electrochemical [5], mechanochemical [6], ionothermal [7], and solvothermal methods

[8]. Regarding the manufacturing of high-yield products, also performing reactions in environmental conditions that the speed of the reaction is performed under favorable conditions, novel methods of ultrasound, reflux, and hydrothermal have been considered recently [9, 10].

5f- series of elements are not only unique due to their radioactivity but also because of different oxidation states and atomic and cationic radius. As uranium, which is the heaviest element of this group, has attracted a lot of attention due to its nuclear physics and chemical status [11].

Among several MOFs made of the uranium, uranyl (UO₂)⁺² is the most common structural unit for this metal [12]. Therefore, the fabricating of uranyl-MOF has a particular importance with regard to its ideal features. These compounds due to their ideal properties in a variety of fields, such as environmental are applicable [13].

The photocatalytic activity is a phenomenon based on the absorption of photons and the formation of electron–hole pairs. These compounds react with molecules present on the surface of the particles [14]. Until the present, a lot of MOFs has been developed due to features such as high surface area, mechano-chemical stability, and high absorption capacity of

✉ Daryoush Afzali
darush_afzali@yahoo.com

¹ Department of Nanotechnology, Graduate University of Advanced Technology, Kerman, Iran

² Environment and Nanochemistry Department, Research Institute of Environmental Science, International Center for Science, High Technology & Environmental Science, Kerman, Iran

³ Department of Material Science and Engineering, Ferdowsi University of Mashhad, Mashhad, Iran

sunlight for photocatalytic activity [15]. But, the main problem with these compounds is the low quantum efficiency of the photocurrent, which leads to the recombination of the electron–hole pairs [16], so the use of new photocatalysts with high efficiency has particular importance.

Phenol red is an environmental pollutant that is categorized in the tribenzo-methane group of dyes. Phenol red has red crystals with a good stability in the aqueous solutions [17]. The toxicity data show that phenol red inhibits the growth of kidney cells and has very harmful effects on health [18].

In this study, the uranyl-MOF was synthesized for the first time using the curcumin ligand by fast and high efficiency reflux, ultrasound, hydrothermal and ultrasound assisted reflux techniques. The 2^{k-1} factorial statistical method was applied to design the parameters affecting the photocatalytic activity as well as the systematic study of the process to degradation of phenol red from aqueous samples.

2 Materials and methods

2.1 Materials

The experimental materials include, curcumin ligand (99% purity, Merck, Germany), uranyl acetate (99% purity, Merck, Germany), ethanol (99.8% purity, Merck, Germany), phenol red (Merck, Germany) and distilled water. All materials were used without further purification.

2.2 Instrument and characterization

The ultrasound apparatus manufacturing company of Bandelin sonopuls (model no: HD3200) was used for synthesis procedure. FT-IR spectrometer (tensor, manufactured by Bruker, Germany), X-ray diffractometer (XRD, Philips, Netherlands), thermogravimetric analysis (model Q600), scanning electron microscopy (SEM, model Em3200, manufactured by China kyky corporation), transmission electron microscopy (TEM, Philips CM120), and N_2 gas adsorption/desorption measurements (Belsrp Mini ii, Bel company, Japan) were utilized in order to acquire characteristic information.

2.3 Uranyl-MOF synthesis

2.3.1 Ultrasound method

The typical method for the synthesis of uranyl-MOF nanostructures by ultrasound route is as follows: first, 0.080 g of uranyl acetate was dissolved in 40 mL distilled water. Also, 0.117 g of curcumin ligand was dissolved in 48 mL of ethanol. Then, the two solutions were mixed, and the

resultant solution was subjected to the ultrasound irradiation of 200 W for 30 min. After 4 days, the red crystals of the uranyl-curcumin-MOF were formed. After this time, in order to evaporate the solvent, the solution was poured into the watch glasses and placed at room temperature. Finally, it was placed in an oven device for 4 h at 200 °C for removal of excess water.

2.3.2 Reflux method

In order to synthesize uranyl-MOF nanostructures with reflux method, the solutions were first prepared according to the sect. 2.3.1. It was then placed under reflux conditions at 50 °C for 4 h. In order to dry the sediment and evaporate the solvent, the solution was poured into the watch glass and placed at room temperature. After collecting the precipitates, the final product was placed at 200 °C for 4 h in an oven device.

2.3.3 Hydrothermal method

After preparing the solution according to the sect. 2.3.1, the solutions were poured into the autoclave and placed in an oven device at 200 °C for 4 h. In order to remove the impurities, the precipitate was placed three times in a centrifuge at a speed of 3000 rpm and each time for 10 min. After each rotation period, the sediment was washed with distilled water and the resulting precipitate was poured into a glass container for drying. Finally, after drying and collecting precipitates, the final product was placed in oven device at 200 °C for 4 h.

2.3.4 Ultrasound assisted reflux method

After preparing the solution under ultrasound conditions, according to the sect. 2.3.1, the solution was placed under reflux conditions according to the sect. 2.3.2.

2.4 Sorption capacity

Sorption capacity of phenol red is determined by using different concentrations of phenol red (5, 25, 35 and 50 mg/L), and catalyst content of (5 g/L) at room temperature in different times (10–70 min) interval by GC–MS device (model Agilent, GC: 6890).

2.5 Degradation of phenol red

First, a solution of phenol red with a certain concentration (5–50 mg/L) was prepared and then, a certain amount of uranyl-curcumin-MOF (0.1–1 mg) was mixed. The mixture was placed in the shaker device in a certain time (5–35 min) in order to completely mixing the materials. Then, this mixture

was centrifuged for 5 min, and after separating the catalyst, spectral solutions were plotted by using visible-ultraviolet spectrometry. Four different experiments were done in various conditions such as, without irradiation, free catalyst, under visible light, and by UV-Vis which is as an irradiation source for a certain period of time.

2.6 Systematic study and RSM optimization

The 2^{k-1} method and RSM optimization were used for experimental design of the procedure. Also, these systematic studies were applied for evaluating the effects of several parameters (pH, contact time, phenol red concentration and photocatalyst content) on the photocatalytic activity of the uranyl-MOF in the degradation of phenol red.

3 Result and discussion

3.1 Suggested formula

FT-IR spectra were used for identifying the functional groups and organic molecules in the composition structure. Figure 1a shows the FT-IR spectrum of the curcumin ligand. Based on this Fig, the observed peaks in the range of 1428.47 – 1596.73 cm^{-1} can be related to the aromatic C=C vibrations. The peaks near 3040.04 and 2940.75 cm^{-1} refer to the stretching vibrations of the C–H aromatic unsaturated bonds. The presence of absorption bands in the range of 1628 cm^{-1} probably indicates the vibrations of C=O bond. Also, the peaks in the range of 3500.02 – 3380.93 cm^{-1} are related to the vibrations of OH groups. These peaks represent the functional groups in the curcumin structure [19].

In Fig. 1b, the FT-IR spectrum of the synthesized uranyl-MOF samples by ultrasound, reflux, hydrothermal and ultrasound assisted reflux techniques has been shown. In four

samples, a new peak appears in the range of 460.96 and 555.58 cm^{-1} , which can be indicative of U–O bonding [20]. According to FT-IR spectra and different configurations of the curcumin ligand [21], the structure of the Fig. 2 is suggested for the formation of uranyl-MOF.

3.2 XRD patterns

The XRD patterns of raw curcumin ligand and uranyl-MOF products are shown in Fig. 3. The new emerged peaks in the products compare to raw curcumin can be related to the formation of a new phase of uranyl-curcumin-MOF. The effects of synthesis routes in the XRD results of the samples (Fig. 3) indicate that ultrasound irradiation causes just the increment in widening of the major peaks. This may come from the effects of new nucleation in preferable sites in the solution. Also, this outcome plays up that the time or power of the irradiation is enough to make such favourable changes [22]. It is seen the minor discrepancy in the hydrothermal patterns than the others in some position ($2\theta = 25.23, 28.37, 31.84, 33.18$), is related to some degeneration of precursors in to subject of higher temperature required for the synthesis procedure. Especially in reflux method, the various diffusion of atoms in the solution are involved that can affect density. There are no significant peak shifts in the patterns. The crystallite size of the synthesized uranyl-MOF samples under different methods is calculated based on Scherer formula (Table 1). Based on the calculated results, it is found that the synthesized samples by ultrasound and ultrasound assisted reflux methods have relatively smaller crystallite sizes than the other methods.

3.3 Thermal gravimetric analysis (TGA)

According to TGA results (Fig. 4), there are two major steps for weighting loss in curcumin precursor. In first step,

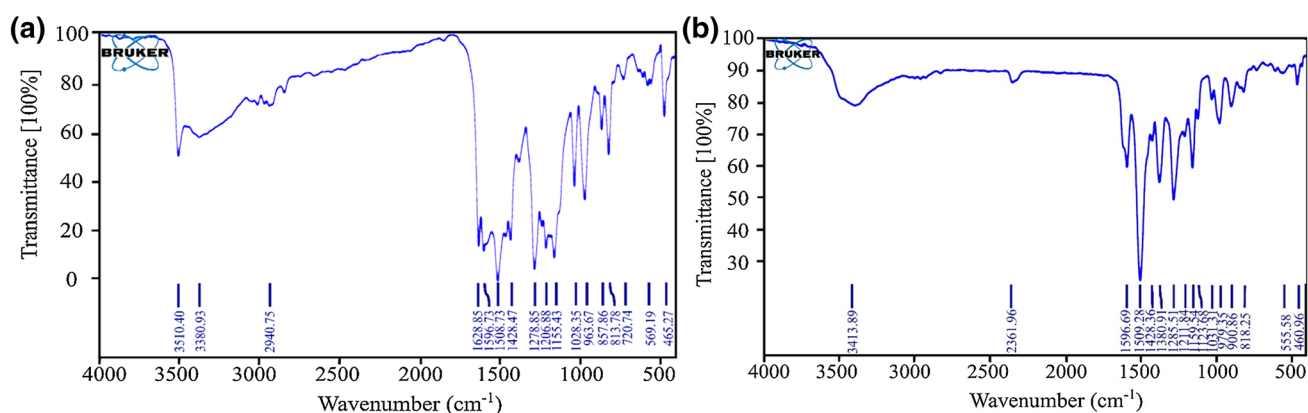


Fig. 1 a The FT-IR spectrum of curcumin ligand, and b the synthesized uranyl-MOF samples by ultrasound, reflux, hydrothermal and ultrasound assisted reflux techniques

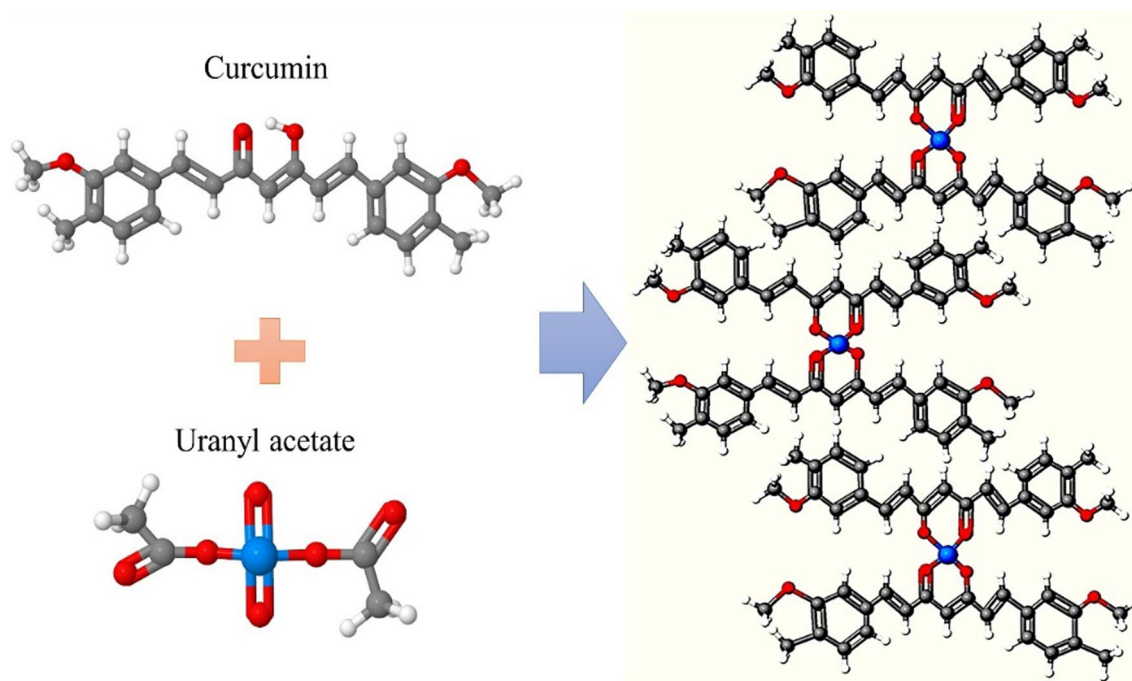


Fig. 2 The suggested formula of the synthesized uranyl-MOF samples by ultrasound, reflux, hydrothermal and ultrasound assisted reflux techniques

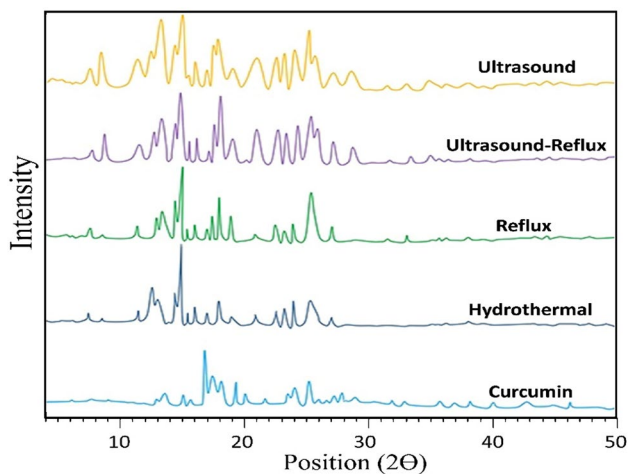


Fig. 3 XRD patterns of the synthesized uranyl-MOF by different methods

Table 1 Average crystallite sizes of the synthesized uranyl-MOF samples by different methods

Method	Average crystallite size (nm)
Ultrasound	9
Reflux	24
Hydrothermal	27
Ultrasound assisted reflux	11

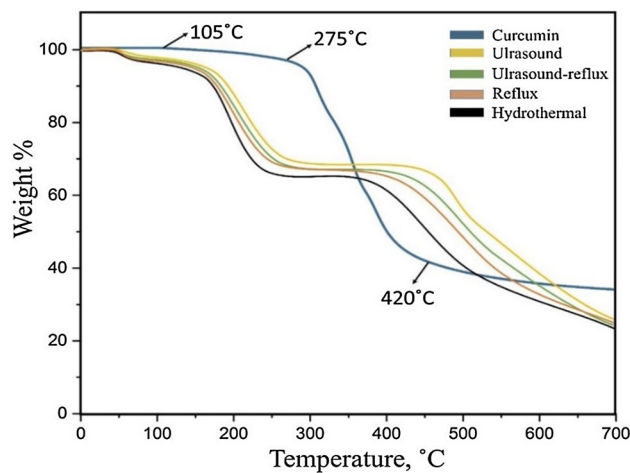


Fig. 4 TGA curve of the synthesized uranyl-MOF by different methods

slightly weight change due to the evaporation of moisture (105 °C) is occurred, and in the later step (275 °C) its structure goes to collapse and cause degenerated. Also, there are two main weight loss levels in the final products of the samples. Firstly, all of them lost their adsorbed water and guest molecules (around 45–250 °C). At last, the frameworks are stable up to 365, 380, 410 and 445 °C, for hydrothermal, reflux, ultrasound assisted reflux and ultrasound methods, respectively. The thermal stability of a MOF is determined

by different factors, such as ligand stability, and also how much the strength between used ligands and metal units specifically their chemical bonding [23]. The facile crystallization of the precursor, the better conjunction between ligand and precursor and also excellent uniform particles distribution could be more achievable in the ultrasound power source than afforded heat in the hydrothermal method. These factors could result in better thermal stability for ultrasound synthesized sample compare to hydrothermal or reflux methods.

3.4 Morphology and size distribution

In this section, the morphology and size of the synthesized uranyl-MOF samples by different methods of reflux, ultrasound, hydrothermal and ultrasound assisted reflux have been investigated by SEM images. Figure 5a, b illustrates the SEM images of the synthesized samples under reflux conditions. Since the average particle size distribution is less than 100 nm, the nanoscale nature of the products is confirmed [24].

SEM images of the synthesized uranyl-MOF samples by ultrasound method (Fig. 5c, d) show that the compounds have a uniform morphology. In this method, the average particle size is in the range of 40–90 nm and agglomeration in the structure is not observed. Also, the particle size distribution of the sample is more uniform than the synthesized sample by the reflux method. The stability of these samples can be attributed to the effects of ultrasound irradiation on the morphology and particle size distribution of the products [25].

Figure 5e shows the SEM image of the synthesized uranyl-MOF samples by ultrasound assisted reflux method, which confirms the nanoscale nature of the samples. The stability of these compounds is higher than the reflux-synthesized samples which cause these structures exhibit less agglomeration. By comparing this image with SEM images of the ultrasound synthesized samples, it is evident that the synthesized sample by ultrasound assisted reflux method is slightly agglomerated which shows the lower stability of this compound [26]. Although the dominant morphology of these structures is spherical, in some parts, the particles are growing in the form of rod shape. This can be due to the use of ultrasound assisted reflux method that affects the morphology of the samples.

Regarding hydrothermal synthesized samples (Fig. 5f), it is evident that these specimens are distributed in the nanoscale and are almost uniform. In this method, the particles aggregated in some areas will be coordinated in the lattice of uranyl-MOF samples. This can be likely attributed to the used solvent in this study. Therefore, a high temperature (about 250 °C) is required to eliminate this solvent [27]. On the other hand, in this study, the hydrothermal method with

a temperature of 190 °C has been used, so it is likely that this water is coordinated as impurities placed in the lattice of metal organic framework nanostructure which may cause structural instability.

As a result, the SEM images showed that ultrasound synthesized samples have more homogeneous morphology and more spherical distribution. Also, morphology and size distribution of the sample synthesized by ultrasound (optimal method) are evaluated by TEM images as depicted in the Fig. 6a, b. As observed the particles have nanosized nature. Also, there is no evidence of the agglomeration in this sample that confirms the result obtained from the SEM image. Indeed, the majority of particles have polygonal shape with a mean diameter range of 35 nm.

3.5 Textural properties

The samples synthesized by ultrasound and ultrasound assisted reflux method because of their better properties compared to the other methods, including higher thermal stability and homogeneous particle size distribution, were selected as desirable products. In order to determine the textural properties of these samples, the N₂ adsorption/desorption isotherms at 77 K were used. Based on the results obtained from Fig. 7a, b, the ultrasound synthesized sample has a surface area of 42.62 m²/g, while the hydrothermal synthesized sample had a surface area of 4.94 m²/g. The results of the BJH method Fig. 8a, b indicating that in both methods, the samples had a mesoporous nature, with an average pore size of 2.74 nm. Also, the N₂ adsorption/desorption isotherms of the synthesized samples by both methods are typical IUPAC type IV form [28]. Based on these results, especially higher surface area for the synthesized samples by ultrasound method compare to other, it is concluded that these samples could be much more effective to have such potentials in order to choose for photocatalytic applications.

3.6 Determining the calibration curve for measuring the phenol red

The calibration curves by acquired absorption amount from different solutions of phenol red at the known concentrations (Table 2) were obtained. By using these data, the concentration of unknown solutions was determined [29]. As shown in Fig. 9, the different absorption amounts versus varying concentrations in the wavelengths of 430 and 580 nm for the phenol red are presented.

3.7 Photoluminescence (PL) spectra

PL spectra at room temperature of the synthesized uranyl-MOF samples by ultrasound, reflux, hydrothermal

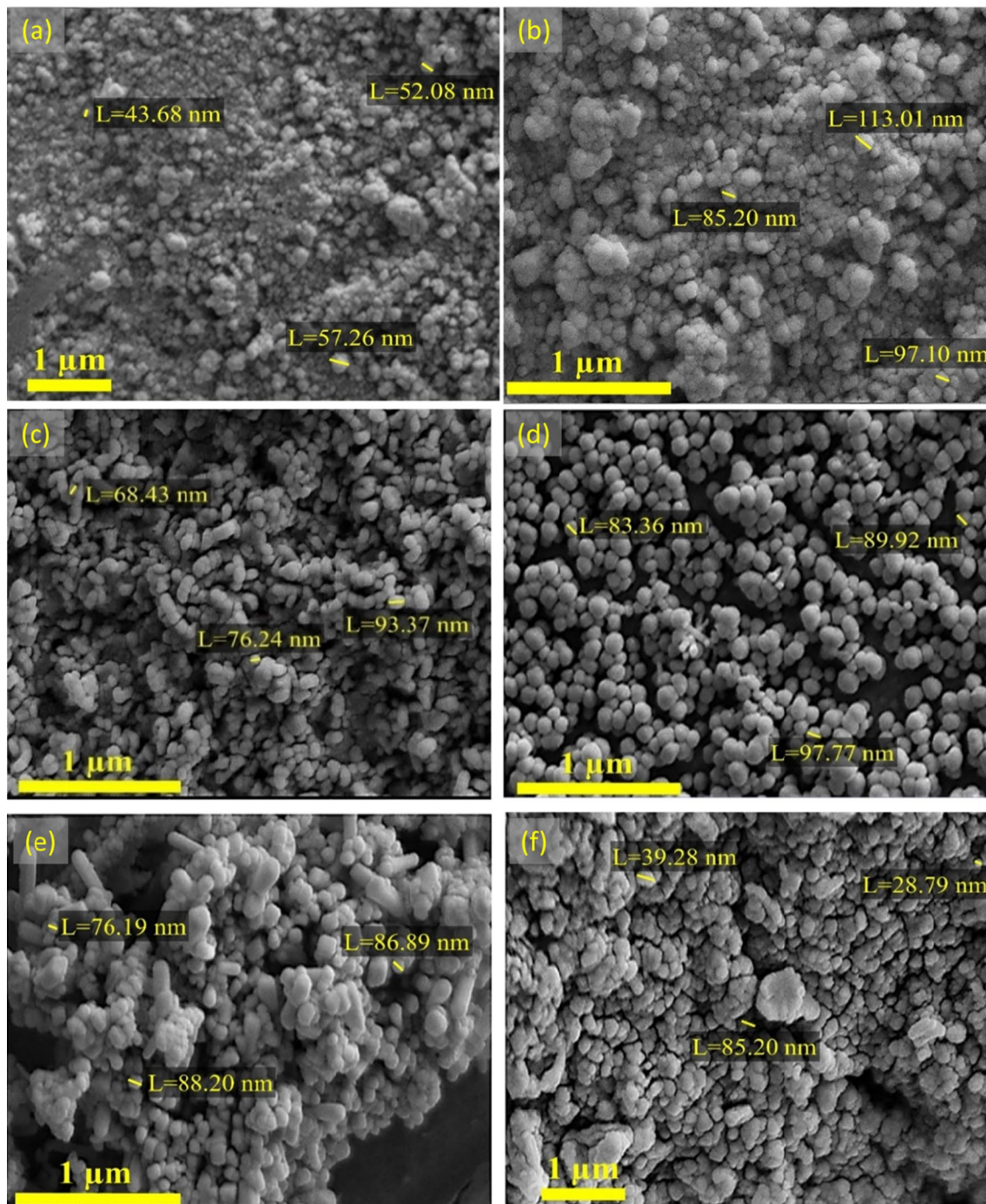


Fig. 5 SEM images of the synthesized uranyl-MOF samples by **a, b** reflux method (different magnifications), **c, d** ultrasound method (different magnifications), **e** ultrasound assisted reflux, and **f** hydrothermal methods

and ultrasound assisted reflux techniques were depicted in Fig. 10. All of them are focused on a main emission band in the range of 495 nm. By comparing these four curves, it is found that the intensity of the synthesized sample by ultrasound method is lower from the other method, and close to the synthesized sample by ultrasound-reflux method. The lower PL intensities for these samples is

caused by lower density surface states that is resulted from lower crystallite size (Table 1) and more fine distribution of small particles (Fig. 6c, d. These unique structural properties for these types of the synthesized samples in favour of ultrasound irradiation indicate higher photocatalytic potential [30, 31].

Fig. 6 TEM images of the synthesized uranyl-MOF sample by ultrasound method at different magnifications

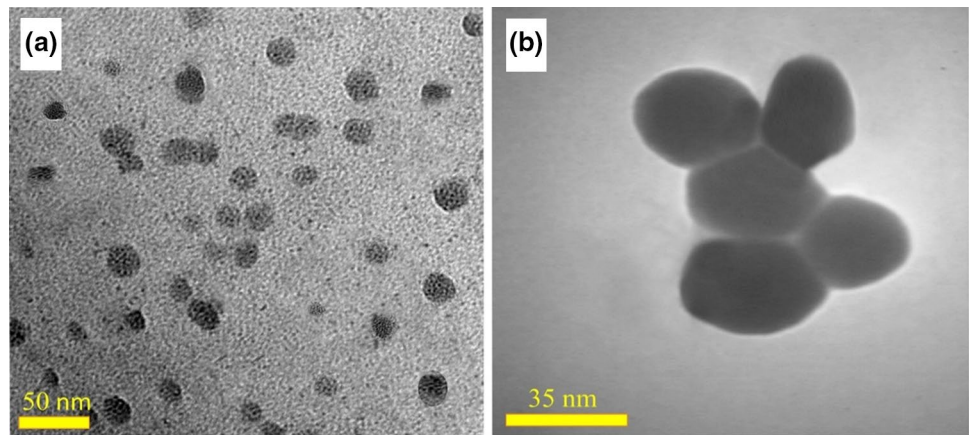


Fig. 7 Pore size distribution of the synthesized uranyl-MOF sample by **a** ultrasound, and **b** ultrasound assisted reflux method

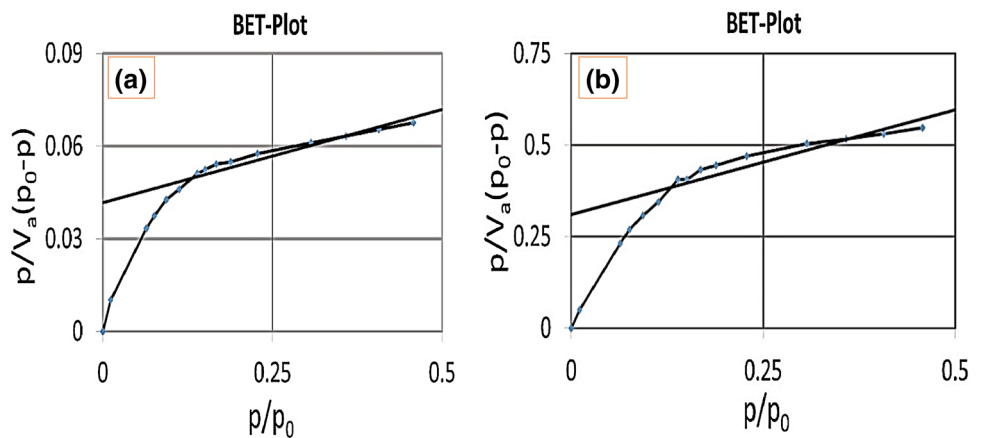


Fig. 8 N_2 adsorption/desorption isotherm of the synthesized uranyl-MOF sample by **a** ultrasound, and **b** ultrasound assisted reflux method

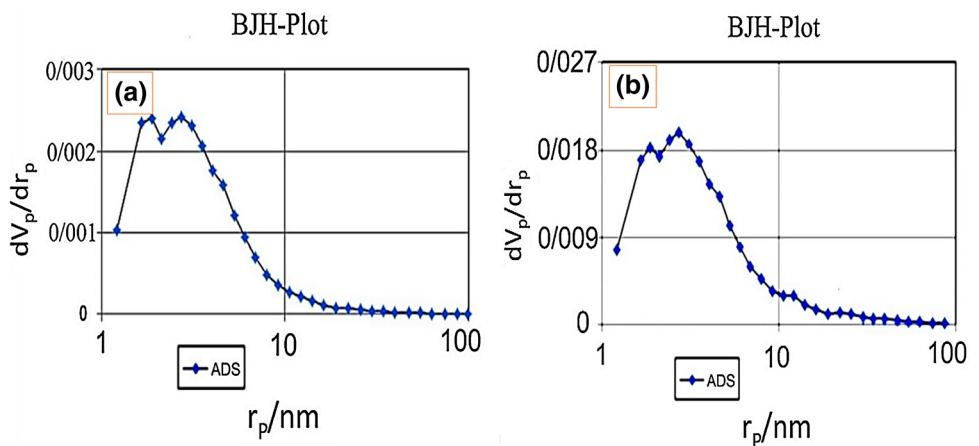


Table 2 The absorptions for different concentrations of phenol red

Concentration (mg/L)	Absorption (nm)
25	0.636
30	0.748
50	0.986

3.8 Sorption capacity

The sorption capacity of the uranyl-MOF sample are depicted in Fig. 11. In all of plots, in early step (about 40 min), there is a steep slope in increasing adsorbate amount of phenol red. However, by increasing time duration, the effect of saturation in sorbent can be seen. Also, by increasing the phenol red concentration, the amount of

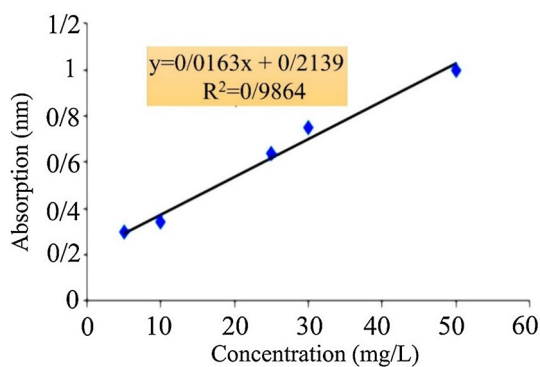


Fig. 9 A standard absorption curve for soluble phenol red

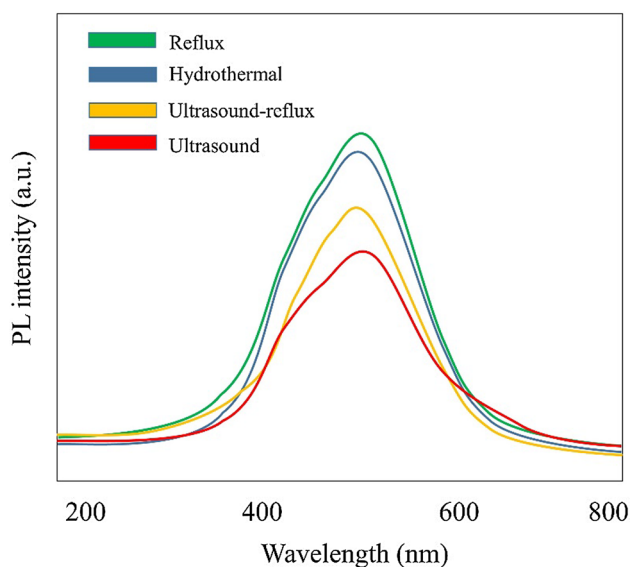


Fig. 10 Photoluminescence spectra of the uranyl-MOF sample synthesized by different methods

q_e will be growth. The highest amount of capacity of sorption (i.e. q_e) equal to 13.84 mg/g will be obtained at initial concentration of phenol red equivalent 50 g/l in a 70 min time of contact.

Photocatalytic activity of the synthesized uranyl-MOF was studied by degrading phenol red in aqueous medium under UV irradiation in different conditions. Band gaps of MOFs determine through the highest occupied molecular orbital (HOMO)- lowest unoccupied molecular orbital (LUMO) gaps of the organic ligand molecule [32]. The proposed mechanism for the degradation of phenol red is that when light falls on photo catalyst result in the excitation of electron (e^-) from valence band to the conduction band of electron creating positively charged hole (h^+) in the valence band of uranyl-MOF. The created hole reacts with H_2O molecules to produce hydroxyl radicals ($\cdot OH$).

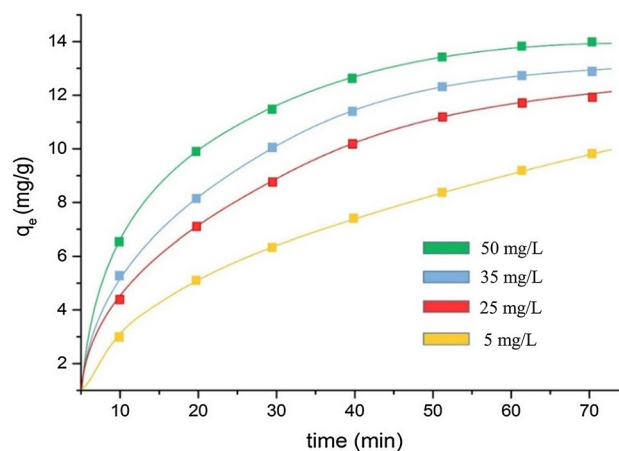
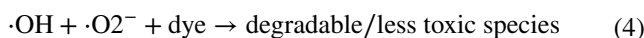
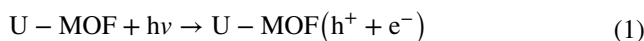


Fig. 11 Sorption capacity of the sample synthesized by ultrasound method as a function of time in a different initial phenol red concentrations (pH 6, catalyst concentration: 5 g/L)

Table 3 The percentage of degradation by uranyl-MOF samples in different conditions

Sample	A	B	C	D
Degradation percent (%)	21	40	35	80

Also, the electron in the conduction band turns the molecular oxygen to superoxide anion radical ($\cdot O_2^-$). These radicals are highly reactive toward phenol red degradation. The major reactions are summarized in the following equations.



In order to investigate the photocatalytic activity of uranyl-MOF in the degradation of phenol red from aqueous samples, an experiment was designed, and the percentage of phenol red degradation in different conditions was studied [33]. At first, four solutions with a specific concentration of phenol red were obtained, samples of A, B, C, D, respectively. Sample A is solution containing phenol red without any irradiation. Sample B contains phenol red with a certain amount of the photocatalyst under the influence of visible light (3 h, 200 W lamp). Sample C is free catalyst under UV irradiation (3 h, 14W lamp), and sample D was the phenol red solution that containing a certain amount of photocatalyst under the influence of UV light (3 h, 14 W lamp). Results indicate the severe impacts

of UV absorbing on the degradation amount of phenol red, and could increase the efficiency about two-fold and this behavior shows that uranyl-MOF is a UV-light activated photocatalyst (Table 3).

3.9 Experimental design

The 2^{k-1} factorial method was used to scientific design of the experiments. Also, it studied the effect of experimental parameters on the photocatalytic behavior of the synthesized uranyl-MOF by ultrasound methods in order to degradation of phenol red from aqueous samples [10]. The four factors investigated include pH (A), contact time (B), phenol red concentration (C) and photocatalyst content (D). Each factor is designed at three levels (Table 4). After designing the experiments with the 2^{k-1} factorial, the samples were carried out experimentally with two replications in the laboratory. The results obtained from degradation of phenol red were reported in Table 5.

Table 4 Coded level ranges from -1 , 0 , $+1$, and uncoded levels of photocatalyst parameters for 2^{k-1} factorial design

Coded levels	Uncoded level of parameters			
	A (pH)	B (min)	C (mg/L)	D (mg)
+1	9	40	0.90	18
0	6	30	0.50	14
-1	3	20	0.10	10

Table 5 The design of the experiments carried out by the 2^{k-1} factorial design, and the responses related to the degradation of the phenol red

Experiment no.	A (pH)	B (min)	C (mg)	D (mg/L)	Rep	Degradation %
a	1	1	1	1	1	40.21
					2	41.02
b	-1	1	-1	1	1	46.60
					2	46.17
c	-1	-1	1	1	1	52.03
					2	51.98
d	1	-1	-1	1	1	74.60
					2	74.87
e	0	0	0	0	1	96.00
					2	97.20
f	-1	-1	-1	-1	1	52.06
					2	52.97
g	1	1	-1	-1	1	87.30
					2	86.14
h	1	-1	1	-1	1	89.69
					2	89.87
i	-1	1	1	-1	1	21.01
					2	20.14

3.9.1 Evaluation of the efficiency of phenol red degradation

In order to verify that the experiments are scientific and the person is not involved in the design and layout of the test, the residual plots of the 2^{k-1} factorial design as output are taken into account [26]. As shown in Fig. 12, there are a number of positive and negative that are equal, and it is demonstrated that the design of the experiments is scientific. In order to investigate the effect of experimental parameters, after designing the experiment with the 2^{k-1} factorial method and entering the experimental data, the results were investigated by analysis of variance [34].

The smaller (p) and higher (α) values imply on the weight of model terms and coefficients (Table 6) [25, 35]. The very low amount of P-value (about 0.000 for all parameters) indicated on the significancy of this model.

Also, Pareto chart (Fig. 13) shows the effect of experimental parameters on the rate of degradation of phenol red. As it is clear, all factors A, B, C, D have a significant effect on the amount of phenol red degradation. Also, this chart illustrates the fact that the interaction of experimental parameter on the effect of degradation is noticeable.

In this study, such general experimental parameters including pH, contact time, concentration and photocatalyst content influenced on the phenol red degradation are in agreement with previous studies [32, 36]. While, in previous studies, to investigate the effects of experimental parameters, the classical process were used which these studies increase

Fig. 12 Residual plots for efficiency of phenol red degradation obtained by 2^{k-1} factorial design

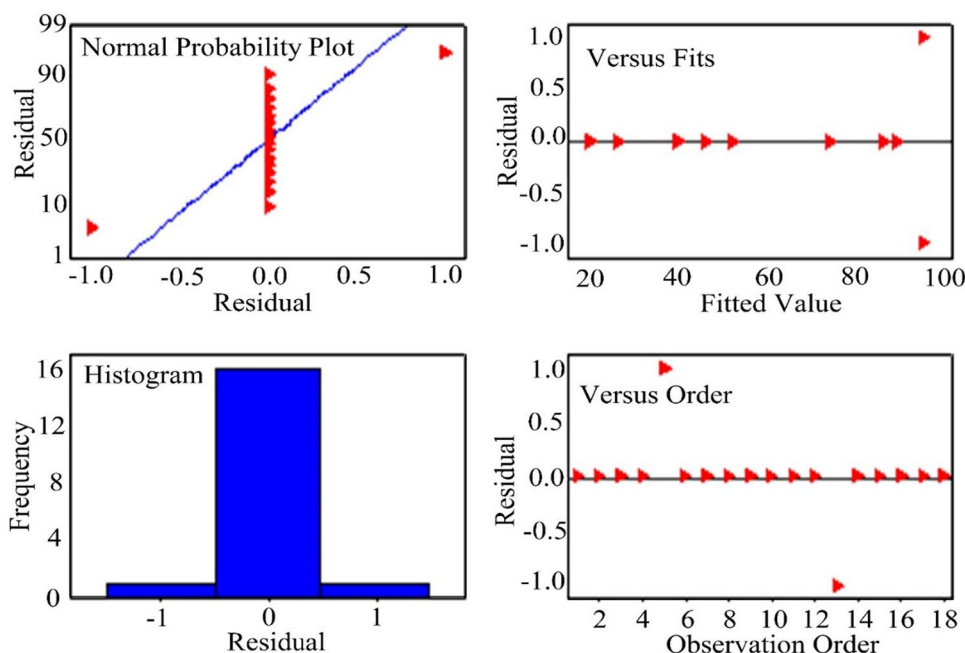


Table 6 Analysis of variance resulting from the effect of experimental parameters on the degradation of phenol red

Source	F _{value}	P _{value}
A	930.25	0.000
B	1722.26	0.000
C	600.25	0.000
D	5256.25	0.000
A*B	156.25	0.000
A*C	110.25	0.000
A*D	930.25	0.000

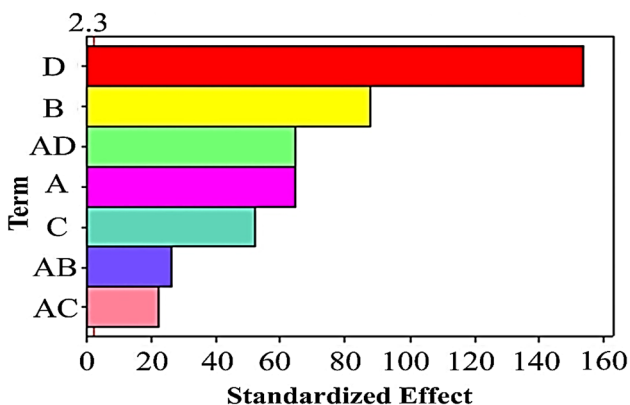


Fig. 13 Pareto chart of the standardized effects according factors A, B, C and D (obtained from the regression model)

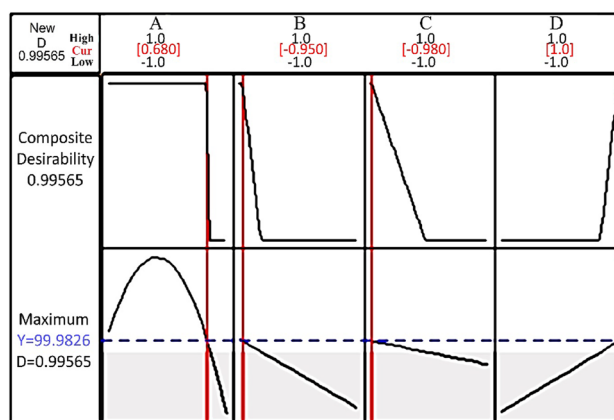


Fig. 14 RSM optimization responses in order to achieve the best degradation efficiency

the number of experiments and, therefore, are not economically feasible also is time-consuming [37, 38].

3.9.2 Optimization of the procedure

Since analysis of variance based on 2^{K-1} factorial design determined the parameters affecting the phenol red degradation, the response surface morphology (RSM) was used to optimize the process and find the best experimental conditions. Since our goal is to achieve the maximum degradation

Table 7 Optimal parameters obtained by 2^{k-1} factorial design (factors are non-coded)

Response	Goal	Lower	Target	Parameters				Desirability	Predict response value
				D (mg)	C (mg/L)	B (min)	A (pH)		
Phenol red degradation (%)	Maximize	99.95	99.99	8.04	11.00	0.11	18.00	0.99	99.98

amount (Fig. 14), the predicted value of the parameters influenced the degradation of the phenol red according to the RSM output that is reported in Table 7. This amount of phenol red degradation acquired by uranyl-MOF has been significantly improved compare with other samples [37, 39, 40]. The high efficiency of these products can be attributed to the development of a novel photocatalyst sample, and the study of various synthesis methods with choice of the appropriate route. Also, the systematic study of the procedure can be led to scientific design of effective parameters that affect the diversity of phenol red degradation in these products. In order to verify the accuracy of the parameters obtained by 2^{k-1} factorial design, the experiment was designed based on optimal parameters (pH 8.04, contact time: 11.00 min, phenol red concentration: 0.11 mg/mL, and photocatalyst content: 18.00 mg), and the percentage degradation was 99%, which indicated the accuracy data obtained by RSM optimization.

Based on what has been investigated, the important factors with effect on the degradation of phenol red from aqueous solutions included pH, contact time, phenol red concentration and photocatalyst content. Also, the ease of production and use of catalysts are vitally important. Based on the Table 8 which summarized similar publications, the main different aspects of this study compare to other researches is fast process and time-saving of degradation by new type of materials developed in this work. Also in this study, the whole process is fast and demand no especial high-cost devices.

3.10 Stability of samples during photocatalytic experiment

One of the restriction in using of photocatalytic materials is related to stability and ability to reusable of these catalysts.

In order to examine this features in the synthesized uranyl-MOF sample by ultrasound method, XRD patterns is done, and result is depicted in Fig. 15. Based on this upshot, we concluded that crystallinity of the structure and also the framework is remain almost unchanged that can be cost-effective and contribute in saving resources.

4 Conclusion

The novel metal–organic framework of uranyl with curcumin ligand was synthesized by ultrasound, reflux, hydrothermal and ultrasound assisted reflux methods. The results showed that the synthesized sample by ultrasound methods, indicated the high surface area, good crystalline structure and also have the lowest agglomeration or any clustering among the particles. These features make the ultrasound irradiation as an efficient and optimum route for production such MOFs. The 2^{k-1} factorial method was used to systematic design and study the effects of experimental parameters on the photocatalytic activity of the synthesized uranyl-MOF by ultrasound methods in the degradation of phenol red from aqueous samples. During the experimental design, different degradation percentages were observed from 20 to 96%, and the optimal parameters (pH 8.04, contact time: 11.00 min, phenol red concentration: 0.11 mg/L and photocatalyst content: 18.00 mg) were determined. According to the optimal parameters, the RSM showed 99.98% of degradation performance. Also stability test showed very good crystallinity and structure preserve even after degradation from synthesized sample by ultrasound method.

Table 8 The summary of previous studies on phenol red degradation by different catalysts

Type of catalyst	Synthesis method	pH	Time (min)	Phenol red con.	Catalyst con.	Irradiation Type	Degradation (%)	REF.
Nanosized TiO ₂	sol–gel	Neutral	100	3.76 × 10 ⁻⁵ M	0.6 g/L	solar	95.2	[41]
Goethite (in PR-GO-H ₂ O ₂ system)	Ageing precipitates	6.9	60	10 ⁵ mol/L	1 g/L	sun light UV 365 nm	98 80	[42]
Multiferroic BiFeO ₃	Hydrothermal	–	120	3.5 mg/L	100 mg/L	Visible light	56.5	[43]
ZnS loaded TiO ₂	Precipitation cum sol gel	6.5	150	3.76 × 10 ⁻⁴ M	6 g/L	UV-A	87.1	[44]
Nanoscale TiO ₂ and ZnO	Reflux	Neutral	240	100 mL aqueous Solution of phenol (5 ppm)	0.05 g	Visible light	47	[45]
Nitrogen-doped TiO ₂ /WO ₃ nano-composite	Solid phase reaction Followed by calcination	5	180	250 ml of PR (50 ppm)	–	Visible UV	93.87 75.74	[46]
Ni-doped niobate/carbon composite	High energy ball milling	–	240	3.53 × 10 ⁻⁵ mol /L	100 ml	UV	85	[47]
Bi ₁₂ O ₁₇ Br ₂ /Bi ₂ O ₃ loaded g-C ₃ N ₄	Hydrothermal	–	80	4 ml	50 mg	Visible	≈ 100	[48]
Zn ₃ V ₂ O ₈ nanostructures	Solvent-free solid-state synthesis	–	150	0.0005 g	0.05 g	UV	65 (bulk precursor) 92 (Nano size Precursor)	[38]
Nanocrystalline TiO ₂	Sol–gel (TiO ₂ + H ₂ O ₂ + O ₂ gas)	4.5	300	5–25 ppm	0.5 g/l	UV	94	[32]
ZnO Nano-particles	Purchased without any treatment	–	60	0.0106 ppm	0.25–3.5 wt%	UV	97	[49]
TiO ₂	Particle size of 30 nm	Neutral	180	10 mg/L	1 g/l	mercury	99.15	[50]
Type ZnO ₂ Cr Core/Shell	Polymeric precursor	acid medium	240	3.53 × 10 ⁵ mol/l	100 mg	UV	61	[40]
		Basic medium	240	3.53 × 10 ⁻⁵ mol/l	100 mg	UV	49	
Red mud and black nickel mud	–	–	60 180	10 ⁻³ mol/dm ³ 10 ⁻³ mol/dm ³	– –	UV UV	77.83 99.53	[51]
TiO ₂	Commercial	9	1440	2 g/L	20 mg/L	UV	94.04	[52]
TiO ₂	Commercial	–	1440	100 ppm	0.9 g/L	UV–C	≈ 100	[53]
Uranyl–cucumin–MOF	Ultrasound method	8	11	0.11 mg/L	0.18 mg	UV	≈ 100	This work

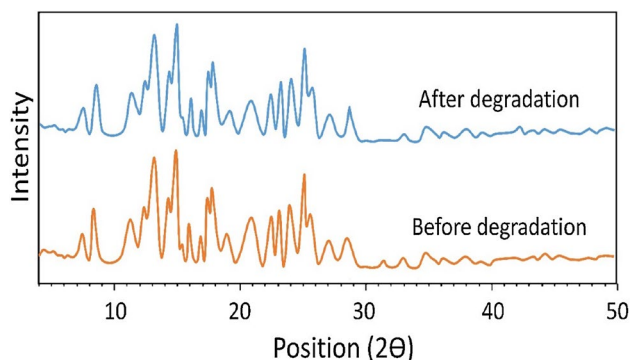


Fig. 15 XRD patterns of the synthesized uranyl-MOF sample by ultrasound method after photocatalytic degradation of phenol red

Acknowledgements The authors would like to acknowledge financial support for this work from the Graduate University of Advanced Technology, Kerman, Iran.

References

1. S. Kitagawa, Metal-organic frameworks (MOFs). *Chem. Soc. Rev.* **43**, 5415–5418 (2014)
2. M. Rosenthal, A. Gabrielli, F. Moore, The evolution of nutritional support in long term ICU patients: from multisystem organ failure to persistent inflammation immunosuppression catabolism syndrome. *Minerva Anesthesiol.* **82**, 84–96 (2016)
3. S. Shahid, K. Nijmeijer, S. Nehache, I. Vankelecom, A. Deratani, D. Quemener, MOF-mixed matrix membranes: precise dispersion of MOF particles with better compatibility via a particle fusion approach for enhanced gas separation properties. *J. Membr. Sci.* **492**, 21–31 (2015)
4. Q. Zhang, J.n.M. Shreeve, Metal-organic frameworks as high explosives: a new concept for energetic materials. *Angew. Chem. Int. Ed.* **53**, 2540–2542 (2014)
5. M. Rubio-Martinez, C. Avci-Camur, A.W. Thornton, I. Imaz, D. Maspoch, M.R. Hill, New synthetic routes towards MOF production at scale. *Chem. Soc. Rev.* **46**, 3453–3480 (2017)
6. D. Lv, Y. Chen, Y. Li, R. Shi, H. Wu, X. Sun, J. Xiao, H. Xi, Q. Xia, Z. Li, Efficient mechanochemical synthesis of MOF-5 for linear alkanes adsorption. *J. Chem. Eng. Data* **62**, 2030–2036 (2017)
7. T.P. Vaid, S.P. Kelley, R.D. Rogers, Structure-directing effects of ionic liquids in the ionothermal synthesis of metal-organic frameworks. *IUCrJ* **4**, 380–392 (2017)
8. F. Abbasloo, S.A. Khosravani, M. Ghaedi, K. Dashtian, E. Hosseini, L. Manzouri, S.S. Khorramrooz, A. Sharifi, R. Jannesar, F. Sadri, Sonochemical-solvothermal synthesis of guanine embedded copper based metal-organic framework (MOF) and its effect on oprD gene expression in clinical and standard strains of *Pseudomonas aeruginosa*. *Ultrason. Sonochem.* **42**, 237–243 (2018)
9. V. Butova, A. Budnyk, E. Bulanova, C. Lamberti, A. Soldatov, Hydrothermal synthesis of high surface area ZIF-8 with minimal use of TEA. *Solid State Sci.* **69**, 13–21 (2017)
10. G. Sargazi, D. Afzali, A. Mostafavi, A novel synthesis of a new thorium (IV) metal organic framework nanostructure with well controllable procedure through ultrasound assisted reverse micelle method. *Ultrason. Sonochem.* **41**, 234–251 (2018)
11. H. Lindner, E. Schneider, Review of cost estimates for uranium recovery from seawater. *Energy Econ.* **49**, 9–22 (2015)
12. S.G. Thangavelu, C.L. Cahill, Uranyl-promoted peroxide generation: synthesis and characterization of three uranyl peroxo [(UO₂)₂(O₂)] complexes. *Inorganic chemistry*, **54** (2015) 4208–4221
13. Y. Wang, Z. Liu, Y. Li, Z. Bai, W. Liu, Y. Wang, X. Xu, C. Xiao, D. Sheng, J. Diwu, Umbellate distortions of the uranyl coordination environment result in a stable and porous polycatenated framework that can effectively remove cesium from aqueous solutions. *J. Am. Chem. Soc.* **137**, 6144–6147 (2015)
14. A.K. Ebrahimi, I. Sheikhshoae, M. Mehran, Facile synthesis of a new metal-organic framework of copper (II) by interface reaction method, characterization, and its application for removal of malachite green. *J. Mol. Liq.* **240**, 803–809 (2017)
15. L. Pan et al., MOF-derived C-doped ZnO prepared via a two-step calcination for efficient photocatalysis. *Appl. Catal. B* **189**, 181–191 (2016)
16. M. Bagheri, M.Y. Masoomi, A. Morsali, A MoO₃-metal-organic framework composite as a simultaneous photocatalyst and catalyst in the PODS process of light oil. *ACS Catal.* **7**, 6949–6956 (2017)
17. O. Yadav, Research article removal of phenol red dye from contaminated water using barley (*Hordeum vulgare* L.) husk-derived activated carbon nigussie alebachew department of chemistry, Haramaya University, PO Box 138, Dire Dawa, Ethiopia. *Sci. Int.*, **5** (2017)
18. N. Mubarak, N. Sazila, S. Nizamuddin, E. Abdullah, J. Sahu, Adsorptive removal of phenol from aqueous solution by using carbon nanotubes and magnetic biochar. *NanoWorld J.* **3**, 32–37 (2017)
19. Y. Liu, D. Ying, Y. Cai, X. Le, Improved antioxidant activity and physicochemical properties of curcumin by adding ovalbumin and its structural characterization. *Food Hydrocoll.* **72**, 304–311 (2017)
20. S.M. Butorin, K.O. Kvashnina, D. Prieur, M. Rivenet, P.M. Martin, Characteristics of chemical bonding of pentavalent uranium in La-doped UO₂. *Chem. Commun.* **53**, 115–118 (2017)
21. J.-H. Zhu, X. Zhao, J. Yang, Y.-T. Tan, L. Zhang, S.-P. Liu, Z.-F. Liu, X.-L. Hu, Selective colorimetric and fluorescent quenching determination of uranyl ion via its complexation with curcumin. *Spectrochim. Acta Part A* **159**, 146–150 (2016)
22. G. Sargazi, D. Afzali, N. Daldosso, H. Kazemian, N. Chauhan, Z. Sadeghian, T. Tajerian, A. Ghafarinazari, M. Mozafari, A systematic study on the use of ultrasound energy for the synthesis of nickel-metal-organic framework compounds. *Ultrason. Sonochem.* **27**, 395–402 (2015)
23. B. Mu, K.S. Walton, Thermal analysis and heat capacity study of metal-organic frameworks. *J. Phys. Chem. C* **115**, 22748–22754 (2011)
24. A.A. Alqadami, M.A. Khan, M.R. Siddiqui, Z.A. Alotman, Development of citric anhydride anchored mesoporous MOF through post synthesis modification to sequester potentially toxic lead (II) from water. *Microporous Mesoporous Mater.* **261**, 198–206 (2018)
25. G. Sargazi, D. Afzali, A. Mostafavi, S.Y. Ebrahimipour, Ultrasound-assisted facile synthesis of a new tantalum (V) metal-organic framework nanostructure: design, characterization, systematic study, and CO₂ adsorption performance. *J. Solid State Chem.* **250**, 32–48 (2017)
26. G. Sargazi, D. Afzali, A. Mostafavi, An efficient and controllable ultrasonic-assisted microwave route for flower-like Ta (V)-MOF nanostructures: preparation, fractional factorial design, DFT calculations, and high-performance N₂ adsorption. *J. Porous Mater.* (2018). <https://doi.org/10.1007/s10934-018-0586-3>
27. J.A. Darr, J. Zhang, N.M. Makwana, X. Weng, Continuous hydrothermal synthesis of inorganic nanoparticles: applications and future directions. *Chem. Rev.* **117**, (2017) 11125–11238

28. Z. Liu, R. Yu, Y. Dong, W. Li, B. Lv, The adsorption behavior and mechanism of Cr (VI) on 3D hierarchical α -Fe₂O₃ structures exposed by (0 0 1) and non-(0 0 1) planes. *Chem. Eng. J.* **309**, 815–823 (2017)
29. K. Liang, R. Ricco, C.M. Doherty, M.J. Styles, S. Bell, N. Kirby, S. Mudie, D. Haylock, A.J. Hill, C.J. Doonan, Biomimetic mineralization of metal-organic frameworks as protective coatings for bi macromolecules. *Nat. Commun.* **6**, 7240 (2015)
30. D.D. Dionysiou, G.L. Puma, J. Ye, J. Schneider, D. Bahnemann, *Photocatalysis: applications* (Royal Society of Chemistry, London, 2016)
31. H. Benhebal, M. Chaib, T. Salmon, J. Geens, A. Leonard, S.D. Lambert, M. Crine, B. Heinrichs, Photocatalytic degradation of phenol and benzoic acid using zinc oxide powders prepared by the sol-gel process. *Alex. Eng. J.* **52**, 517–523 (2013)
32. H.S. Wahab, A.A. Hussain, Photocatalytic oxidation of phenol red onto nanocrystalline TiO₂ particles. *J. Nanostr. Chem.* **6**, 261–274 (2016)
33. M. Shishkin, D. Volkov, I. Pelivanov, M. Proskurnin, Direct solubility determination in optically dense solutions of highly soluble chromophores by the optoacoustic technique: acidity dependence for phenol red. *Anal. Chim. Acta* **953** (2017) 57–62
34. A.P. Simezo, C.E. da Silveira Bueno, R.S. Cunha, R.A. Pelegrine, D.G.P. Rocha, A.S. de Martin, A.S. Kato, Comparative analysis of dentinal erosion after passive ultrasonic irrigation versus irrigation with reciprocating activation: an environmental scanning electron study. *J. Endod.* **43**, 141–146 (2017)
35. G. Sargazi, D. Afzali, A. Mostafavi, S.Y. Ebrahimipour, Synthesis of CS/PVA biodegradable composite nanofibers as a microporous material with well controllable procedure through electrospinning. *J. Polym. Environ.* (2017) 1–14
36. L. Xu, W. Sun, L. Zhang, M. Zhang, Y. Wang, S. Yu, Facile synthesis of α -Fe₂O₃/diatomite composite for visible light assisted degradation of Rhodamine 6G in aqueous solution. *J. Mater. Sci.* **28**, 4661–4668 (2017)
37. M. Ghiyasiyan-Arani, M. Salavati-Niasari, M. Masjedi-Arani, F. Mazloom, An easy sonochemical route for synthesis, characterization and photocatalytic performance of nanosized FeVO₄ in the presence of aminoacids as green capping agents. *J. Mater. Sci.* **29**, 474–485 (2018)
38. F. Mazloom, M. Masjedi-Arani, M. Salavati-Niasari, Rapid and solvent-free solid-state synthesis and characterization of Zn₃V₂O₈ nanostructures and their phenol red aqueous solution photodegradation. *Solid State Sci.* **70**, 101–109 (2017)
39. W. Jiang, J. Yang, X. Wang, H. Han, Y. Yang, J. Tang, Q. Li, Phenol degradation catalyzed by a peroxidase mimic constructed through the grafting of heme onto metal-organic frameworks. *Bioresour. Technol.* **247**, 1246–1248 (2018)
40. G.S. Silveira, M.A. Nobre, S. Lanfredi, Photodegradation of Phenol Red in a Compound of Type ZnO₂Cr Core/Shell. *Mater. Sci. Forum* **881**, 410–415 (2017)
41. A.M. Asiri, M.S. Al-Amoudi, T.A. Al-Talhi, A.D. Al-Talhi, Photodegradation of Rhodamine 6G and phenol red by nanosized TiO₂ under solar irradiation. *J. Saudi Chem. Soc.* **15**, 121–128 (2011)
42. S. Belattar, N. Debbache, I. Ghoul, T. Sehili, A. Abdessemed, Photodegradation of phenol red in the presence of oxyhydroxide of Fe (III)(Goethite) under artificial and a natural light. *Water Environ. J.* <https://doi.org/10.1111/wej.12333>
43. R. Dhanalakshmi, M. Muneeswaran, N. Giridharan, Effect of synthesis conditions on the photocatalytic property of multiferroic BiFeO₃ towards the degradation of phenol red. In: *AIP Conference Proceedings*, (AIP Publishing, 2016), p. 130016
44. G. Sargazi, D. Afzali, A.K. Ebrahimi, A. Badoei-dalfard, S. Malekabadi, Z. Karami, Ultrasound assisted reverse micelle efficient synthesis of new Ta-MOF@ Fe₃O₄ core/shell nanostructures as a novel candidate for lipase immobilization. *Mater. Sci. Eng. C* **93**, 768–775 (2018)
45. S. Janitabar Darzi, M. Movahedi, Visible light photodegradation of phenol using nanoscale TiO₂ and ZnO impregnated with merbromin dye: a mechanistic investigation. *Iranian J. Chem. Chem. Eng. (IJCCE)* **33**, 55–64 (2014)
46. T. Teka, A. Tadesse, Effect of selected operating parameters on the photocatalytic efficiency of nitrogen-doped TiO₂/WO₃ nano-composite material for photodegradation of phenol red in aqueous solution. *Int. J. Innovat. Appl. Stud.* **7**, 174 (2014)
47. S. Lanfredi, M.A. Nobre, P.G. Moraes, J. Matos, Photodegradation of phenol red on a Ni-doped niobate/carbon composite. *Ceram. Int.* **40**, 9525–9534 (2014)
48. X. Lin, S. Jiang, Z. Lin, M. Wang, Y. Yan, The influence of g-C₃N₄ loading on the photocatalytic activity of Bi₁₂O₁₇Br₂/Bi₂O₃ composite in the phenol red degradation. In: *IOP Conference Series: Materials Science and Engineering*, (IOP Publishing, 2016), p. 012020
49. T. Tan, P. Khiew, W. Chiu, S. Radiman, R. Abd-Shukor, N. Huang, H. Lim, Photodegradation of phenol red in the presence of ZnO nanoparticles. *World Acad. Sci. Eng. Technol.* **79**, 791–796 (2011)
50. N. Laoufi, D. Tassalit, F. Bentahar, The degradation of phenol in water solution by TiO₂ photocatalysis in a helical reactor. *Glob. NEST J.* **10**, 404–418 (2008)
51. B. Galbičková, M. Soldán, M. Belčík, K. Balog, Removal Of phenol from wastewater by using low-cost catalyst from metal production. *Res. Pap. Fac. Mater. Sci. Technol. Slovak Univ. Technol.* **22**, 55–59 (2014)
52. H. Hamdi, A. Namane, D. Hank, A. Hellal, Coupling of photocatalysis and biological treatment for phenol degradation: application of factorial design methodology. *J. Mater.* **8**, 3953–3961 (2017)
53. D. Trinh, S. Le, D. Channei, W. Khanitchaidecha, A. Nakaruk, Investigation of intermediate compounds of phenol in photocatalysis process. *Int. J. Chem. Eng. App* **7**, 273–276 (2016)